

A low-energy ion spectrometer with half-space entrance for three-axis stabilized spacecraft

[RenXiang HU](#), [Xu SHAN](#), [GuangYuan YUAN](#), [ShuWen WANG](#), [WeiHang ZHANG](#), [Wei QI](#), [Zhe CAO](#), [YiRen LI](#), [ManMing CHEN](#), [XiaoPing YANG](#), [Bo WANG](#), [SiPei SHAO](#), [Feng LI](#), [XiaoQing ZHONG](#), [Dan FAN](#), [XinJun HAO](#), [ChangQing FENG](#), [ZhenPeng SU](#), [ChengLong SHEN](#), [Xin LI](#), [GuYue DAI](#), [BingLin QIU](#), [ZongHao PAN](#), [Kai LIU](#), [ChunKai XU](#), [ShuBin LIU](#), [Qi AN](#), [TieLong ZHANG](#), [YuMing WANG](#) and [XiangJun CHEN](#)

Citation: [SCIENCE CHINA Technological Sciences](#) **62**, 1015 (2019); doi: 10.1007/s11431-018-9288-8

View online: <http://engine.scichina.com/doi/10.1007/s11431-018-9288-8>

View Table of Contents: <http://engine.scichina.com/publisher/scp/journal/SCTS/62/6>

Published by the [Science China Press](#)

Articles you may be interested in

[Accelerometer error estimation and compensation for three-axis gyro-stabilized camera mount based on proportional multiple-integral observer](#)

[SCIENCE CHINA Technological Sciences](#) **57**, 2387 (2014);

[Analyzing the antenna pointing error of three-axis stabilized geostationary satellite](#)

[SCIENTIA SINICA Physica, Mechanica & Astronomica](#) **41**, 589 (2011);

[A manifold approach to generating iso-scallop trajectories in three-axis machining](#)

[SCIENCE CHINA Technological Sciences](#) **54**, 131 (2011);

[Modal solutions in stratified multi-layered fluid-solid half-space](#)

[Science in China Series D-Earth Sciences](#) **45**, 358 (2002);

[Determination of DNA single-strand breaks by low-energy heavy ion and analysis of dose-effect curves](#)

[Chinese Science Bulletin](#) **44**, 711 (1999);

A low-energy ion spectrometer with half-space entrance for three-axis stabilized spacecraft

HU RenXiang¹, SHAN Xu^{1*}, YUAN GuangYuan², WANG ShuWen², ZHANG WeiHang³,
 QI Wei³, CAO Zhe², LI YiRen³, CHEN ManMing³, YANG XiaoPing⁴, WANG Bo⁴,
 SHAO SiPei⁴, LI Feng⁵, ZHONG XiaoQing⁵, FAN Dan⁵, HAO XinJun³, FENG ChangQing²,
 SU ZhenPeng³, SHEN ChengLong³, LI Xin³, DAI GuYue³, QIU BingLin³, PAN ZongHao³,
 LIU Kai³, XU ChunKai¹, LIU ShuBin², AN Qi², ZHANG TieLong³, WANG YuMing^{3*}
 & CHEN XiangJun¹

¹Hefei National Laboratory for Physical Sciences at the Microscale, Department of Modern Physics,
 University of Science and Technology of China, Hefei 230026, China;

²State Key Laboratory of Particle Detection and Electronics (IHEP-USTC), Department of Modern Physics,
 University of Science and Technology of China, Hefei 230026, China;

³CAS Key Laboratory of Geospace Environment, School of Earth and Space Sciences,
 University of Science and Technology of China, Hefei 230026, China;

⁴Shandong Institute of Space Electronic Technology, Yantai 264003, China;

⁵Institute of Telecommunication Satellite, China Academy of Space Technology, Beijing 100094, China

Received March 5, 2018; accepted May 14, 2018; published online October 19, 2018

A low-energy ion spectrometer (LEIS) for use aboard three-axis stabilized spacecraft has been developed to measure ion energy per charge distribution in three-dimensional space with good energy-, angular- and temporal-resolutions. For the standard top-hat electrostatic analyzer used widely in space plasma detection, three-axis stabilized spacecraft makes it difficult to obtain complete coverage of all possible ion arrival directions. We have designed angular scanning deflectors supplementing to a cylindrically symmetric top-hat electrostatic analyzer to provide a half-space field of view as $360^\circ \times 90^\circ$ (-45° – $+45^\circ$), and fabricated the LEIS flight model for detecting magnetospheric ions in geosynchronous orbit. The performance of this payload has been evaluated in detail by a series of simulation and environmental tests, and the payload has also been calibrated through laboratory experiments using a low-energy ion source. The results show that capabilities of the LEIS payload are in accordance with the requirements of a magnetospheric mission.

low-energy ion spectrometer, three-dimensional measurement, top-hat electrostatic analyzer, angular scanning deflectors, simulation, ground calibration

Citation: Hu R X, Shan X, Yuan G Y, et al. A low-energy ion spectrometer with half-space entrance for three-axis stabilized spacecraft. *Sci China Tech Sci*, 2019, 62: 1015–1027, <https://doi.org/10.1007/s11431-018-9288-8>

1 Introduction

Plasmas in space, particularly those around magnetized planets, exhibit complex behaviors that are usually measured

by energy spectrometers through detecting electrons and ions from several eV to a few tens of keV kinetic energies. Since space plasmas vary both temporally and spatially, time-resolved three-dimensional (3D) measurements are essential for a comprehensive understanding of plasma processes and behaviors. The hemispherical top-hat electrostatic analyzer

*Corresponding authors (email: xshan@ustc.edu.cn; ymwang@ustc.edu.cn)

(ESA) proposed by Carlson et al. [1] and the toroidal top-hat ESA introduced by Young et al. [2] were widely used for detecting space plasmas in most missions such as Wind [3], Giotto [4], Venus Express [5], Cluster [6,7], FAST [8], etc. Since such a hemispherical or toroidal top-hat ESA (referred to hereafter as standard top-hat ESA) has a structure with rotational symmetry, it has good detecting uniformity in the plane perpendicular to the axis of symmetry. Moreover, the top-hat structure is able to keep a low noise level as ultraviolet photons and neutral particles injected along the plane will just pass through the ESA. Although it has a 360° field of view (FOV) in the azimuthal direction, its FOV in the elevation direction is usually as narrow as several degrees. The necessary 3D coverage is then achieved by the spin of the spacecraft. In this case a single instrument can sequentially sample all directions while the time resolution will be limited to the spacecraft spin period. But on three-axis stabilized spacecraft, it meets a big challenge to obtain complete coverage of all possible ion arrival directions. In order to realize three-dimensional FOV on three-axis stabilized spacecraft. One option is to deploy multiple standard top-hat ESAs so that necessary angular directions can be simultaneously observed, which brings about the complexity in uniform calibrations and requires more resources from the spacecraft such as power, mass, volume and so on. Another option is to deploy the standard top-hat ESA on a rotation table, for example, CAPS on CASSINI [9] and ASPERA-3 on Mars Express [10], which also requires more spacecraft resources. The third option is to broaden the entrance of the standard top-hat ESA in the elevation direction with electrostatic deflectors, which requires additional sweeping high voltage power supplies. Recently, three-axis stabilized spacecraft is favored in most of space missions due to the affinity with imaging instruments. Considering the limited resource of spacecraft, it is quite important to develop lightweight, low-power consuming and compact low-energy charged particle analyzers for 3D measurements.

In this article, we present the development of a miniaturized low-energy ion spectrometer (LEIS) for use aboard three-axis stabilized spacecraft. We attach angular scanning deflectors to a cylindrically symmetric top-hat ESA to provide a half-space FOV as 360°×90°(−45°+45°), which allows it to measure the 3D energy per charge distribution of ions. The LEIS is designed for a magnetospheric spacecraft on geosynchronous orbit, an important region to understand the ring current and outer radiation belt and monitor the space weather. The scientific objectives and required capability of the LEIS are presented in the next section.

2 Scientific objectives and required capability

The geosynchronous orbit, located at a geocentric distance of

$6.6R_E$ in the geographical equatorial plane, roughly corresponds to the outer part of the ring current. The ring current carried by hot (1–100 keV) ions drifting around the Earth is a critical external source of the geomagnetic field [11]. These ring current ions are mainly transported from the magnetotail into the inner magnetosphere [12–14]. Assuming that the first and second adiabatic invariants are conserved in the transport process, we can estimate the distribution of ring current ions in $L < 6.6$ from the observations at $L = 6.6$, which is useful for space weather monitoring and early warning. Previous theoretical and observational works have suggested that the ring current ions can destabilize magnetosonic and electromagnetic ion cyclotron waves [15,16]. These plasma waves potentially contribute to the acceleration and loss of radiation belt electrons [17–19]. On the basis of the measured three-dimensional energy distributions of hot ions, we may also analyze the associated wave instabilities and understand the complex dynamics of outer radiation belt.

The above scientific objectives require a mission possessing the capability to measure three-dimensional energy per charge distributions of these hot ions on a three-axis stabilized spacecraft. Our low energy ion spectrometer focuses on the ions with the energy between 100 eV and 15 keV. Based on the observations from the Van Allen Probes, twin spacecraft launched on 30 August 2012 to research evolution of the radiation belt and ring current around the Earth, the proton fluxes in the energy range from 1 eV to 50 keV can be estimated [20,21]. The orbits of the spacecraft are low inclining and highly elliptical (perigees $\sim 0.1R_E$, apogees $\sim 6R_E$ and periods ~ 9 h) [22]. Although their orbits are different from the geosynchronous orbit, they do frequently cross the L shell of 6.6 near the equatorial plane. By investigating the proton flux data from 2013 to 2015, we find that the lower boundary of the flux varies from 2×10^3 to $1 \times 10^4 \text{ s}^{-1} \text{ cm}^{-2} \text{ sr}^{-1} \text{ keV}^{-1}$ within the energy range of 100 eV–15 keV as shown in Figure 1. To have good energy resolution and also gain sufficient count rates, the energy range is divided into 64 energy bins with 8.5% increment step by step. Then the lower boundary of the integrated flux is about $10^3 \text{ s}^{-1} \text{ cm}^{-2} \text{ sr}^{-1}$. According to the typical performance of a microchannel plate, the dynamic range of the count rate can cover 5 orders. Thus, the instrument is designed to meet the flux range of 10^3 – $10^8 \text{ s}^{-1} \text{ cm}^{-2} \text{ sr}^{-1}$. Note that the upper boundary of the flux range is much higher than the expected flux (see Figure 1), and therefore some extremely large events may still be properly recorded. The main parameters of the LEIS instrument required by the mission are listed in Table 1.

3 Design of the analyzer

According to requirements of the mission, the LEIS is de-

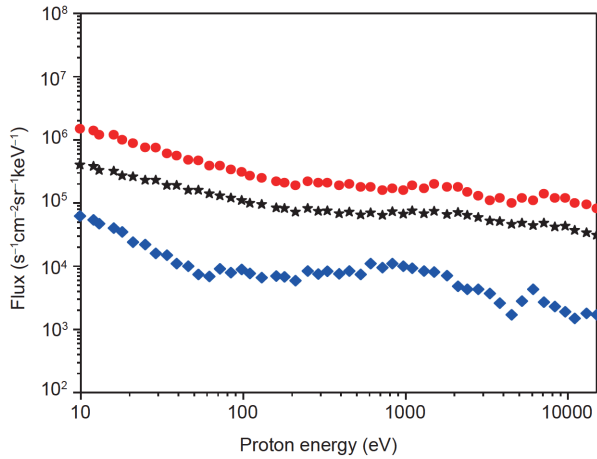


Figure 1 (Color online) Energy dependent proton fluxes observed by Van Allen Probes at $L=6.6$ during 2013–2015. Asterisks denote the averaged energy spectrum, bounded by the top and bottom 5% records.

signed to possess the capabilities to measure three-dimensional energy per charge distributions of magnetospheric ions from 100 eV to 15 keV on a three-axis stabilized spacecraft. This makes us choose the structure combining the top-hat ESA and angular scanning deflectors in the design to achieve a half-space FOV as $360^\circ \times 90^\circ$ and a suitable geometric factor with the same or better angle and energy resolutions as those of the standard top-hat ESA described in the literature. Meanwhile, considering the limited resource of spacecraft, the power consumption, weight, and size should cost as low as possible.

Figure 2 presents the structural schematic diagram of the top-hat ESA with angular scanning deflectors, in which typical particle trajectories are drawn to indicate azimuth-angle focusing, elevation-angle selection and wide ion acceptance. As shown in Figure 2, the analyzer employed in the LEIS has three concentric spherical section elements: an inner sphere (with radius R_1), an outer sphere (with radius R_2), and a small “top-hat” section (with radius R_3). A collimator is formed by two parallel electrodes around the aperture of concentric spherical section elements. In order to extend the FOV, two

pieces of deflecting electrodes, formed by the circle (with radius R_4) rotating for 360° around z -axis, are introduced to form the entrance. At the exit of analyzer, a position sensitive detector (PSD) composed of a pair of annular microchannel plates (MCPs) and an anode plate with 16 discrete anodes is placed on the focal plane. The chevron configuration of MCPs is employed to provide a saturated gain of 10^7 typically, with a narrow pulse height distribution. The discrete anodes have a high strip current to ensure fast counting capability. Note that the angle to axis y in the x - y plane is defined as azimuth angle α , and the angle to the x - y plane is denoted as elevation angle β , as shown in Figure 2(b) and (c), respectively.

When the analyzer is working, the outer sphere, top hat and collimator electrodes are grounded, while the inner sphere and deflector electrodes are applied voltages. The former voltage is for the energy analysis of ions and the latter is for the elevation angle analysis. After deflection through deflecting electrodes and inner sphere, ions with specific kinetic energy and incoming angle will hit the MCP placed at the exit of analyzer, and then the charge pulse amplified via MCP is collected with the anode. The elevation angles of ions are selected by scanning the voltage of deflectors with the range from -45° to $+45^\circ$. The azimuth angles are dependent on 16 discrete anodes, each corresponding to 22.5° .

It is well known that the property of an ESA is closely related to its geometric parameters and the voltages applied. In order to achieve a good performance and match the requirement of the mission, the detailed optimization on geometric parameters has been carried out by using a software package named Simion (<http://simion.com>). After optimization, the geometric parameters are finally given as follows: $R_1=35$ mm, $R_2=38$ mm, $R_3=41$ mm, $R_4=18$ mm, $\theta=15.6^\circ$ and $\sigma=5^\circ$, so $\Delta R=R_3-R_2=R_2-R_1=3$ mm.

4 Simulation of the analyzer’s performance

The analyzer introduced above has been studied in details

Table 1 Main parameters of the LEIS spectrometer

Main parameters	Requirements	Capability
Energy range	100 eV–15 keV	100 eV–15 keV
Energy flux range ($\text{cm}^{-2} \text{sr}^{-1} \text{s}^{-1}$)	10^3 – 10^8	10^3 – 10^8
Energy resolution ($\Delta E/E$)	15%	$\leq 13\%$
Field of view (azimuth angle \times elevation angle)	$360^\circ \times 90^\circ$	$360^\circ \times 90^\circ (-45^\circ - 45^\circ)$
Angular resolution (azimuth angle \times elevation angle)	$22.5^\circ \times 15^\circ$	$\leq 22.5^\circ \times 8^\circ$
Time resolution	64 s	64 s(3D)/2 s(2D)
Geometric factor ($\text{cm}^2 \text{sr eV/eV}$) for each channel	$\sim 10^{-3}$	$\sim 1.0 \times 10^{-3}$
Power	≤ 15 W	~ 8 W
Weight	≤ 10 kg	5.6 kg
Envelope size	$\leq 300 \text{ mm} \times 300 \text{ mm} \times 300 \text{ mm}$	246.7 mm \times 262 mm \times 247 mm

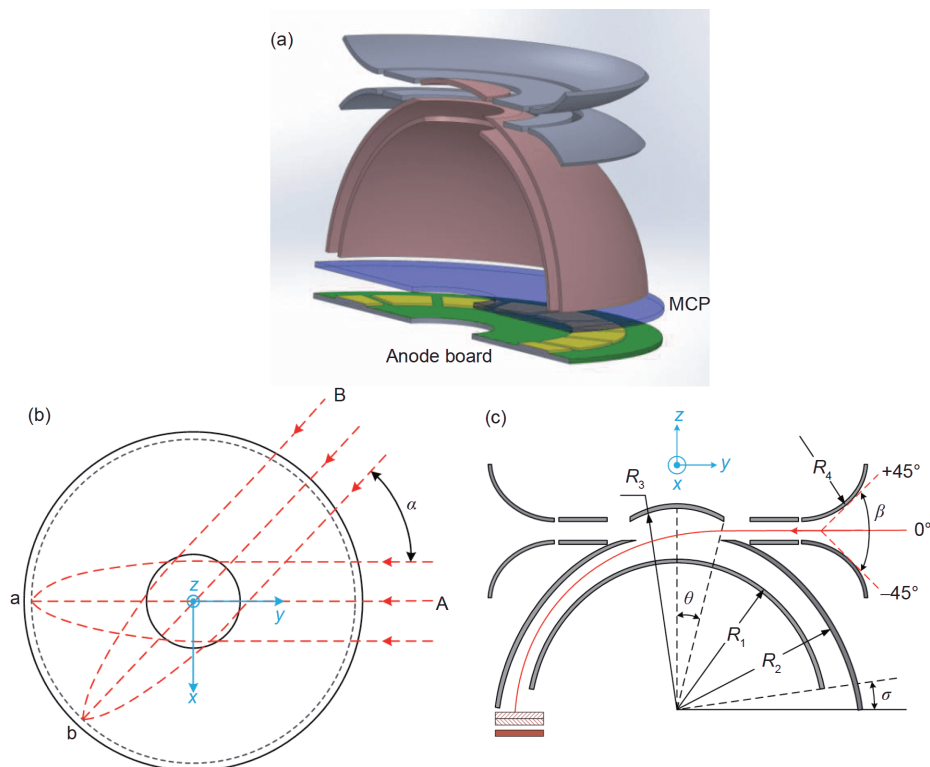


Figure 2 (Color online) Schematic diagram of the top-hat ESA with angular scanning deflectors. (a) Three-dimensional cut-away view; (b) top view; (c) cross-sectional view. Typical particle trajectories are drawn to indicate azimuth-angle focusing, elevation-angle selection and wide ion acceptance.

through simulations using Simion software package (<http://simion.com>). An ion beam (proton) is launched upstream of the analyzer's entrance in the simulation. The ion source used here is a rectangle source with uniform distribution in position. For all small position units, ions are conically emitted along the same established angular direction with small angular spread in an increment of 0.25° one by one. And all ions have a Gaussian distribution in energy with 30% energy spread. The azimuth angle α of the ion beam is always kept as 0° , because of the rotational symmetry of the analyzer. By studying the counts of transmitted ions from different positions with different energy and elevation angles, we obtain the performance parameters of the analyzer. It is noted that the voltage applied to the inner sphere is defined as U_{inner} , and those for the two electrodes of angular scanning deflector as U_{def1} and U_{def2} . The voltage between the two deflecting electrodes is $U_{\text{def}}=U_{\text{def1}}-U_{\text{def2}}$.

4.1 Parameters without entrance deflection

In this section, we set $U_{\text{def1}}=U_{\text{def2}}=0$ to ensure there is no deflection from deflecting electrodes. We firstly research the response of ion energy to the voltage of inner sphere, i.e., the relation between ion energy and spherical deflecting voltage. In the simulation, the β of incident ion beam is given by uniform distribution centering at 0° . Energetic ions with the variable range from 50 eV to 40 keV transmitted to the exit

of the ESA through the selection of a series of specific voltage on the inner sphere. Figure 3(a) shows the energy response for a series of U_{inner} , and the peak shapes are almost the same for different U_{inner} in the simulation. From the energy response spectra in Figure 3(a), we can obtain the energy resolution of the ESA being 12.7%, as shown in Figure 3(b). Similarly, we also get that the analyzer constant K is 5.93 through fitting the ratio of the E/q of ions which pass through the analyzer to the corresponding U_{inner} as shown in Figure 3(c). It is worthwhile to note that the analyzer constant K is a key parameter which enables one to know the energy of detected ions through the sphere voltage.

There is another key parameter called Geometric Factor (GF) [2,23,24]. GF is used as a catch-all term that describes the analyzer transmission rate, representing the sensitivity of ESA. This factor relates the count rate measured to the incident ion energy flux J :

$$\text{Count rate} = GF \times J. \quad (1)$$

GF can be estimated by the formula introduced by [2]

$$GF = A_e \times \left\langle \Delta\beta \times \frac{\Delta E}{E} \right\rangle \times \int \cos\alpha d\alpha, \quad (2)$$

where A_e is the active area, i.e., the area of transmitted ions upstream of the analyzer aperture, $\Delta\beta$ is the elevation angle resolution, $\Delta E/E$ is the energy resolution and α is the azimuth angle. A_e can be estimated by the product of the effective length of ion entrance, X_{FWHM} , and the gap between two

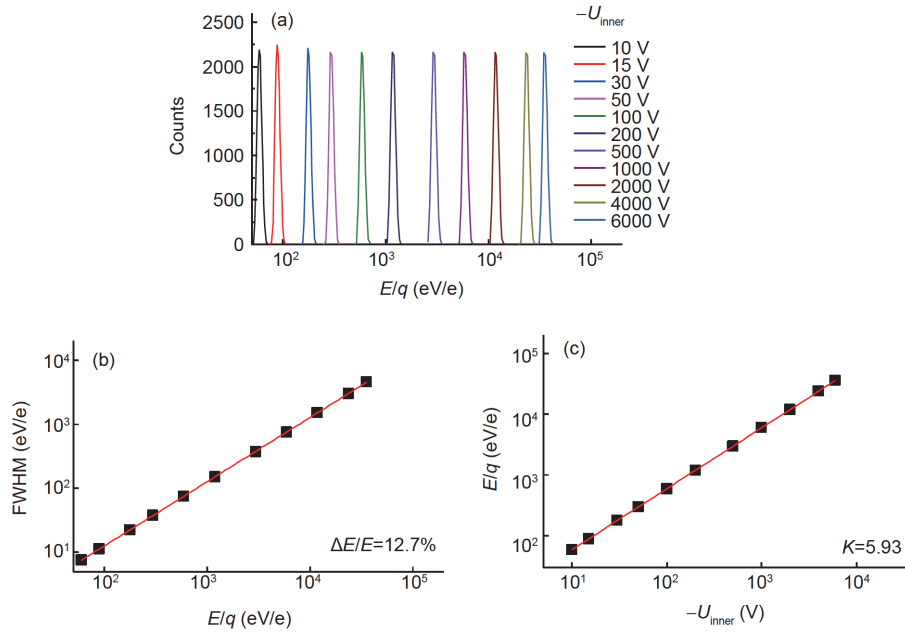


Figure 3 (a) Energy response spectrum; (b) energy resolution; (c) analyzer constant K .

sphere shells, ΔR , as follows:

$$A_e \approx X_{FWHM} \times \Delta R. \quad (3)$$

In order to get the GF , the parameters in eqs. (2) and (3) are demanded to be determined. So we also simulated the azimuth and elevation angular responses, as well as the entrance position of ions. Figure 4(a) shows the beam spot of the transmitted ions at the exit of ESA which has a size of about 20° in azimuth angle. Figure 4(b) presents the corresponding

azimuth angular spectrum, and the resolution of azimuth angle is determined to be 10.8°. Figure 4(c) illustrates the entrance position spectrum of the incident ions, and the effective length of ion entrance position is determined to be 13.6 mm. Figure 4(d) displays that the response spectrum of ions for variable elevation angles around $\beta=0^\circ$, and the resolution is about 4.4°. Taking $\Delta R=3$ mm it gives the active area $A_e=40.8$ mm². So the GF factor for each 22.5° azimuth angle channel can be obtained according to eq. (2) as follows:

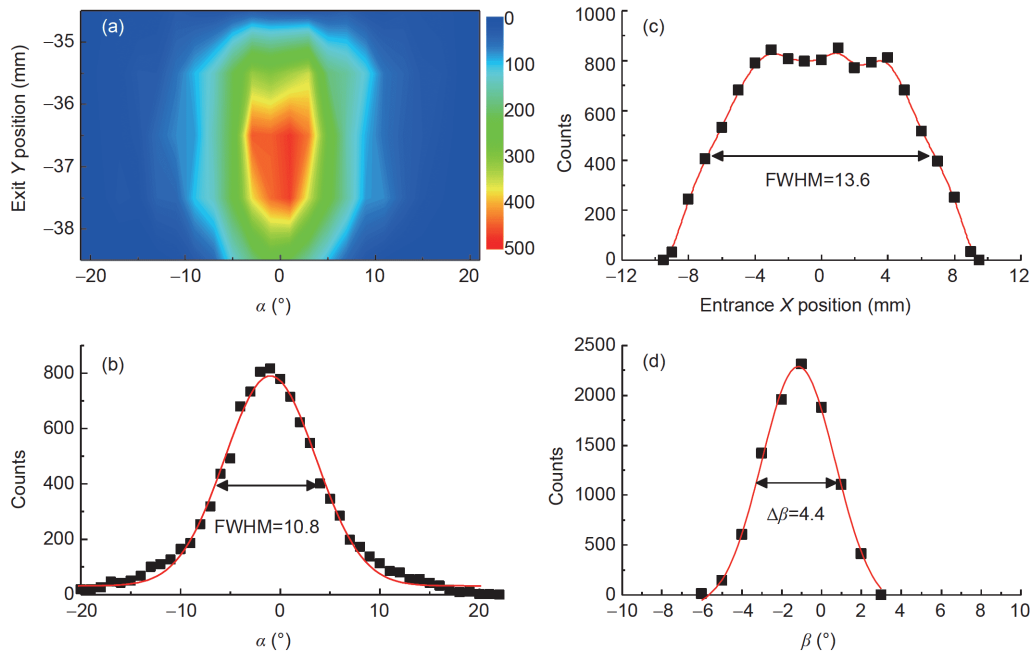


Figure 4 (a) Spot of the transmitted ions at the exit of ESA; (b) azimuth angle response; (c) entrance position of the incident ions; (d) elevation angle response. X and Y represent the directions of coordinate axes as defined in Figure 2.

$$GF = 40.8 \text{ mm}^2 \times 4.4^\circ \times 0.127 \times \int_{-11.25^\circ}^{11.25^\circ} \cos \alpha d\alpha \quad (4)$$

$$\approx 1.56 \times 10^{-3} \text{ cm}^2 \text{ sr eV/eV.}$$

4.2 Parameters with entrance deflection

In order to obtain analyzer responses for different deflecting angle β (elevation angle) of incident ions, entrance deflectors should be applied voltages. In all situations with deflection, we set the voltages satisfying $U_{\text{def}1} = -U_{\text{def}2}$, so the entrance deflecting voltage $U_{\text{def}} = 2U_{\text{def}1} = -2U_{\text{def}2}$.

4.2.1 Energy responses

Figure 5(a) shows the energy response spectra for different ion energies and different elevation angles β . One can see that the responses for different ion energies and angles are almost the same except for the intensity differences of spectra in the terminal large β angles. Such intensity differences are easily understandable according to the different resolutions of energy or angles and different transmission efficiency for these terminal elevation angles.

Similar to Figure 3, we can get the energy resolution and the analyzer constant K for each β from Figure 5(a). Figure 5(b) and (c) shows the variations of the energy resolution and the analyzer constant K with elevation angle β . The energy resolution varies from about 9% to 13% for $-45^\circ \leq \beta \leq 45^\circ$, and it is almost constant for $-30^\circ \leq \beta \leq 30^\circ$. The analyzer constant K keeps good uniformity for $-45^\circ \leq \beta \leq 45^\circ$.

4.2.2 Deflection characteristic

The elevation angle (β) of the detected ions is determined by

the entrance deflector voltage U_{def} and the energy E/q of the ions. Figure 6(a) shows the analyzer response with different $U_{\text{def}}/(E/q)$. The resolution of the elevation angle is therefore estimated as shown in Figure 6(d). In the simulation, the incident ion beam is given as a parallel beam with different β from -50° to 50° with the interval of 10° . From Figure 6(b), we can get the relation between elevation angle and $U_{\text{def}}/(E/q)$, which can be fitted well by a linear function:

$$\beta = 99.82 \frac{U_{\text{def}}}{E/q} + 1.96. \quad (5)$$

Obviously, this functional relation plays an important role in determining the elevation angle of specific energy ions according to the sweeping voltage. In other words, if the voltages of entrance deflectors and the inner sphere are given, the energy and elevation angle of incident ions can be derived with a resolution of elevation angles better than 8° as shown in Figure 6(d). In addition, from the simulated elevation angular spectra in Figure 6(a), the normalized geometric factors for different elevation angles of incoming ions are extracted and plotted in Figure 6(c). In general, they are approximately uniformity relative to that at $\beta=0^\circ$ ($1.56 \times 10^{-3} \text{ cm}^2 \text{ sr eV/eV}$). Using these GF factors and the measured counts rates, one can deduce the energy flux of ions along any given direction of azimuth and elevation angles from the count rates recorded at the exit of the analyzer.

5 Realization of the LEIS spectrometer

The LEIS spectrometer is realized by co-operating the above

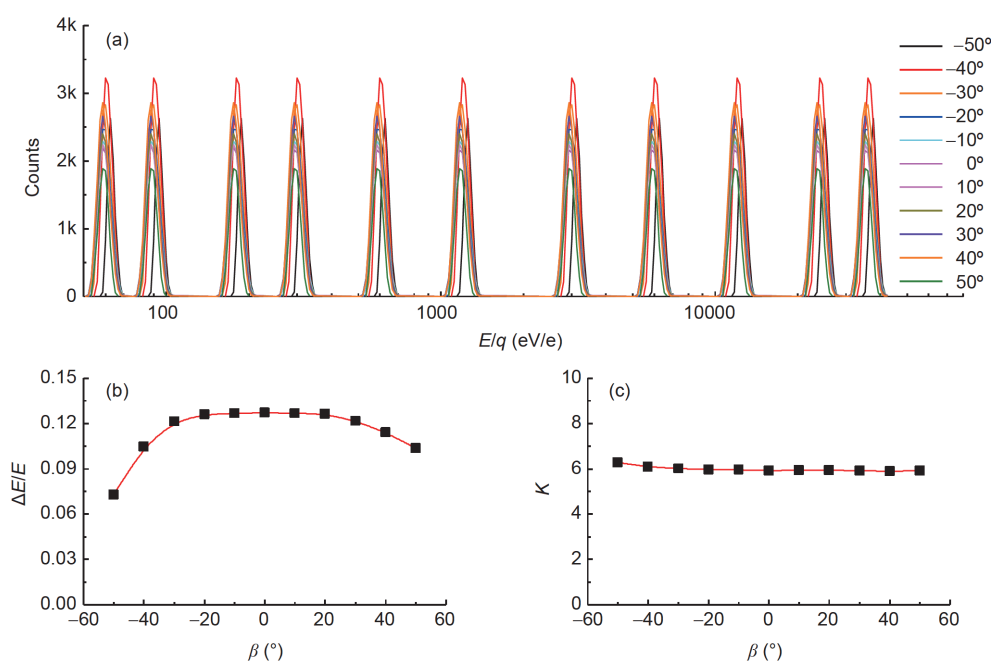


Figure 5 (a) Energy response spectra with different β ; (b) energy resolution ratio; (c) analyzer constant K .

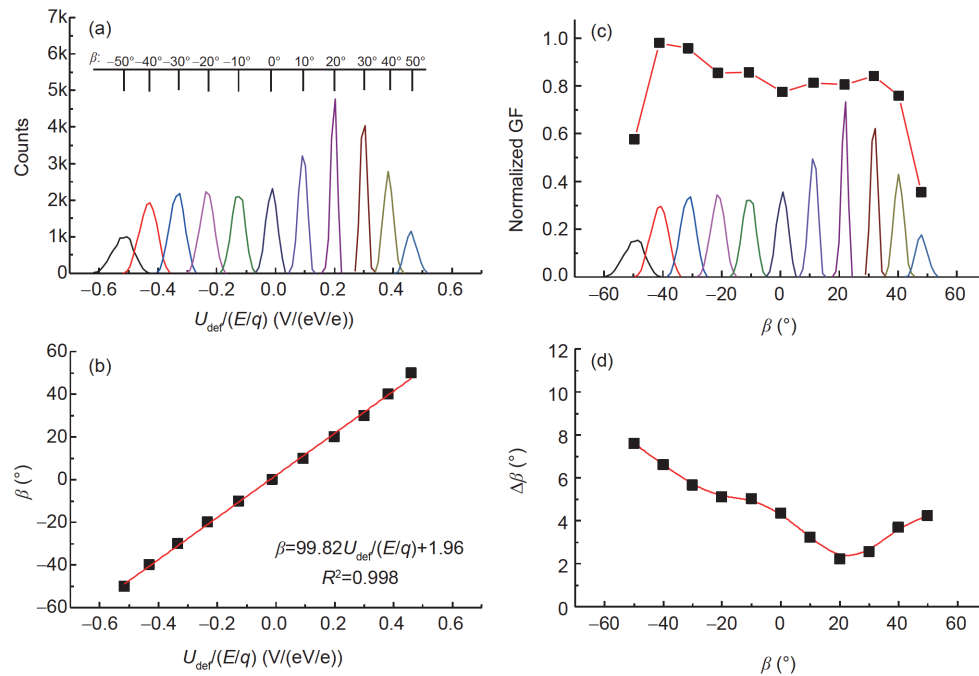


Figure 6 (a) Response spectra of ions at different β with the change of $U_{def}(E/q)$; (b) relation between β and $U_{def}(E/q)$; (c) the normalized GF at different β ; (d) the resolution of elevation angles.

analyzer with an electronic system. Figure 7 presents its functional block diagram and the photograph of the completed LEIS after intergration. The electronic system consists of a digital processing unit (DPU) with signal readouts, a high voltage (HV) power supply unit and a secondary power supply unit (LV), which are divided into three circuit boards: a DPU board, a HV board and a LV board. Signals from each of the 16 anodes are sent through 16 very fast A121 charge-sensitive amplifier/discriminators that are able to count at rates as high as 5 MHz. Note that A121 chips can be remotely adjusted the threshold of the input signal via a reference voltage. The Radiation resistance based DPU is designed to rely primarily on the Field Programmable Gate Array (FPGA) for data acquisition and processing, HV control, analog monitor and communication. The HV board includes three sweeping HV and one fixed HV power supplies. Two sweeping bipolar supplies are applied to the entrance upper and lower deflector electrodes. The other sweeping negative HV is applied to the inner sphere while the outer sphere is grounded. The fixed negative HV is designed for the MCP supply. Optocouplers cooperating with negative and positive HV modules are employed to achieve the sweeping and fixed HV outputs, which is widely used in space instruments. The secondary power supply board transfers a primary power supply offered by the satellite to

several low voltages supplied to electronic system. Detailed design and performance test of the HV and the DPU will be presented in future papers^(1,2). It is noted that the re-programmable tables located in the DPU can control all HV outputs, as well as the sweep steps and the stay time at each step, which can be adjusted via RS422 instructions. An EEPROM is applied to store all values of the parameter of different HVs. In addition, a 4 M bits SRAM on the board is applied to store the data of the spectrometer. By instructions, the data transfer mode can alter either in the real-time mode or in the block mode. A low voltage differential signal (LVDS) channel is employed to upload scientific data to the satellite based on a user-defined serial protocol. The project employs a RS422 channel to receive instructions from the satellite, and respond to the satellite.

In order to meet various requirements of the mission, we have designed two operation schemes for the LEIS flight model. One is the self-test mode, which is used for pre-flight or in-flight calibration tests of the electronic system. For this purpose, a built-in self-test circuit is designed in which a manmade pulse is produced by the capacitive coupling of the adequate analog voltage from a digital-to-analog converter (DAC) chip, and a narrow signal enables the analog switch to turn off or on. Such a pulse generator circuit can stimulate the 16 amplifiers that are under the FPGA control. In this

1) Zhang W H, Hao X J, Li Y R, et al. Development of high-voltage power supply board for a novel low-energy ion spectrometer. Nucl Sci Tech, 2018, submitted.

2) Yuan G Y, Cao Z, Wang S W, et al. Design of the readout electronics for a low-energy ion spectrometer in the space. Nucl Sci Tech, 2018, submitted.

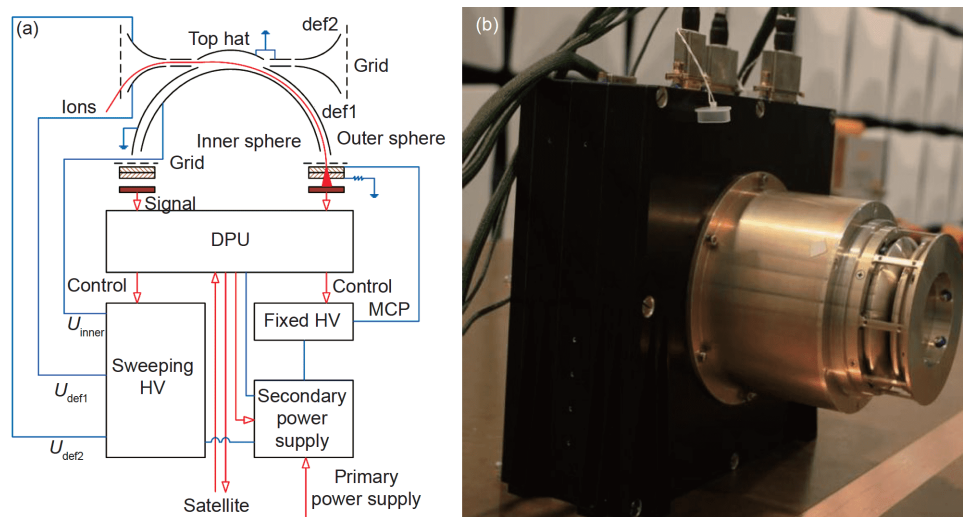


Figure 7 (Color online) (a) Functional block diagram of the LEIS; (b) photograph of the completed LEIS after intergration.

way, important functions of the instrument and of the associated on board processing can easily be tested. In addition, the sweeping high voltage can be tested by measuring the voltage value of each individual step, and the MCP gain can be checked by occasionally stepping MCP HV and by adjusting the discrimination level of the charge amplifiers. Within this program all important functions of the electronics and the subsequent on-board processing of the data can be automatically tested. The in-flight calibration can also be triggered by ground command in a very flexible way.

The other operation scheme is used for the normal measurement, which includes two work modes. One mode is working without entrance deflection, in which we keep $U_{\text{def1}} = U_{\text{def2}} = 0$ and only sweep U_{inner} . In this way, we can measure

the ion energy spectra from 100 eV to 15 keV at 16 azimuth angle channels with high time resolution. The energy range from 100 eV to 15 keV corresponds to the sweeping HV range of U_{inner} from -15 V to -2500 V. we set 64 sweeping steps (i.e., energy bins) as a cycle with exponential change of U_{inner} voltages. Default setting for each voltage step stays 30 milliseconds (ms), it will cost two seconds to obtain 16 azimuthal ion energy spectra up to 15 keV/q. The other mode is working with entrance deflection, in which the voltages of U_{inner} , U_{def1} and U_{def2} are swept synchronously as shown in **Figure 8**. This measurement should be done with as many energies and elevation angles as possible, but this directly impacts the elementary accumulation time and thus the accumulated counts per bin. A trade-off must be found to ob-

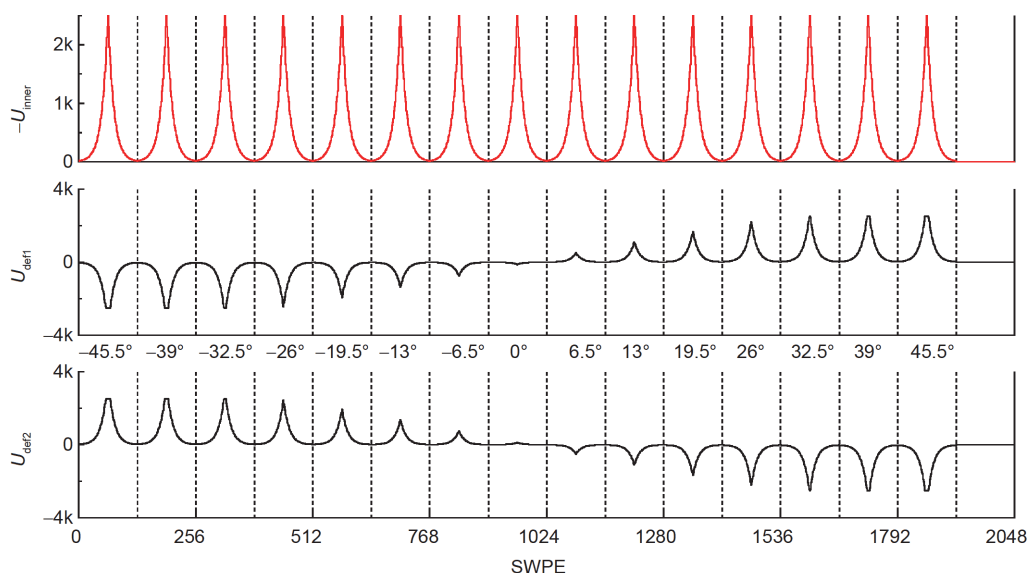


Figure 8 (Color online) Chronogram with 2048 steps in $-U_{\text{inner}}$, U_{def1} and U_{def2} .

tain high time, energy, and angular resolutions, together with a good coverage of the 3D distribution and a good statistic. For this purpose, we devise 64 basic energy bins with 8.5% increment step by step covering a range of order 100 eV–15 keV, 15 elevation angle bins with the angle range from -45° to 45° , and one zero voltage bin for ultraviolet response and background measurements. In order to maintain a constant viewing angle while scanning energy, the deflection and ESA voltages would have to be scanned simultaneously in a fixed ratio. Figure 8 presents the voltage stepping scheme. For each elevation angle, the voltages of U_{inner} , U_{defl} and U_{defz} are swept synchronously in a fixed ratio as the simulation. Each of them takes 128 steps as a minor cycle, which consists of 64 upward sweeping steps and 64 downward sweeping steps. Sweeping of all voltages with an exponential change for a whole period needs 2048 steps. If each step stays 30 ms to sample counts, the time for a complete angle and energy range measurement will be about 64 s. According to the specific science requirements, we can select different operation modes, and set different sweeping step number (e.g., 32 or 64 steps) and sample time at each step (e.g., 16 or 64 ms) through ground command. It is noted that due to the limitation of the maximal output voltage of deflector HV supplies and derating requirements (± 2500 V), for high energy ions over 11 keV/q the measurement can not reach the full coverage of the $\pm 45^\circ$ elevation angle range. For example, for 15 keV/q ions, the actual elevation coverage is about -26° to $+26^\circ$.

In the realization of the LIES spectrometer, besides the detailed designs and tests of the sensor and electronic system presented above, the mechanical design, thermal design, electromagnetic compatibility (EMC), and radiation tolerance, etc., are also carried out carefully according to the construction standard of space instruments. Each of components are manufactured and assembled into a number of sub-assemblies. After further integration, the LIES spectrometer is produced as shown in Figure 7(b). Subsequently, complete engineering experiments have been done for the LEIS flight model, including mechanical test, thermal vacuum experiment, EMC test, etc. The LEIS shows great stability in experiments, and it meets the requirement for space exploration.

6 Calibration of the LEIS spectrometer

Calibration of space-based instruments on the ground is vital to understand the instrumental response characteristic and performance before flight, which lays the foundation for the analysis and proper interpretation of measured data. Preflight calibration of the LEIS flight model was performed at our newly developed vacuum test facility, using the variable energy ion beams produced by an electron impact ion source

in the Institute of Modern Physics at Lanzhou. The test facility consists of a beam expansion lens, a moveable large area MCP-based imaging detector, a 3-axis turntable, a Faraday cup (FC), a vacuum chamber with pump system and the specific ground support system that interfaces to the spectrometer. The lens is used to expand the ion beam spot in order to completely cover the LEIS entrance, and the imaging detector placed in front of the LEIS entrance is employed to record a spatial profile and uniformity of the beam at the beginning and end of the test. The FC with 6 mm inner diameter positioned behind the LEIS entrance is used to measure the current of ion beam through the entrance aperture without deflection. The 3-axis turntable rotates the spectrometer to choose the specific azimuth and elevation angles for calibration, respectively. In the present experiment, the chamber vacuum is better than 2×10^{-5} Pa, and the 1–20 keV proton beam with very small energy spread and a known current is delivered. Considering the limitation of the beam time, we firstly test all flight commands and modes to confirm proper instrument operation, select MCP matching voltage to get a proper gain level, and set the threshold value of amplifiers, etc. After these, the procedure of calibration experiments is divided into two parts: one is that the elevation angle is fixed near zero (i.e., without entrance deflection) while the beam energy is incremented. The other is that the beam energy is fixed while the elevation angle is varied (i.e., with entrance deflection).

6.1 Working without entrance deflection

In this working mode, we set the scanning voltage applied to entrance deflectors off (i.e., choose the ions injected the entrance along the elevation angle $\beta=0^\circ$), and sweep the voltage of inner sphere to measure the energy responses at 16 azimuth angles and a series of proton beam energies. Consequently, many energy response spectra are obtained at different energy and azimuth angles, as well as the corresponding parameters such as energy resolution ratio and analyzer constant. Therefore only a part of spectra are presented here. Figure 9 shows the U_{inner} response for different azimuth angle α (channel 00–15 are serial numbers of anodes, each of which corresponds to 22.5° azimuth angle, covering $0-360^\circ$ range) as the energy of ions is 1554 eV. We can find that the analyzer works well and shows good consistency for different azimuth angle with simulations. Figure 10(a) shows the U_{inner} response for different ion energies at azimuth angle $\alpha=0^\circ$ (i.e., channel 08). One can see that the energy resolution ratio is better than 14% for each of ion energies with the averaged value of 12.6% and the analyzer constant is $K=5.82$, as shown in Figure 10(b) and (c), respectively. Figure 11 shows the analyzer constant K for all 16 channels. The error bars in the figure represent the energy resolutions measured at the specific ion energies. It can be seen that the

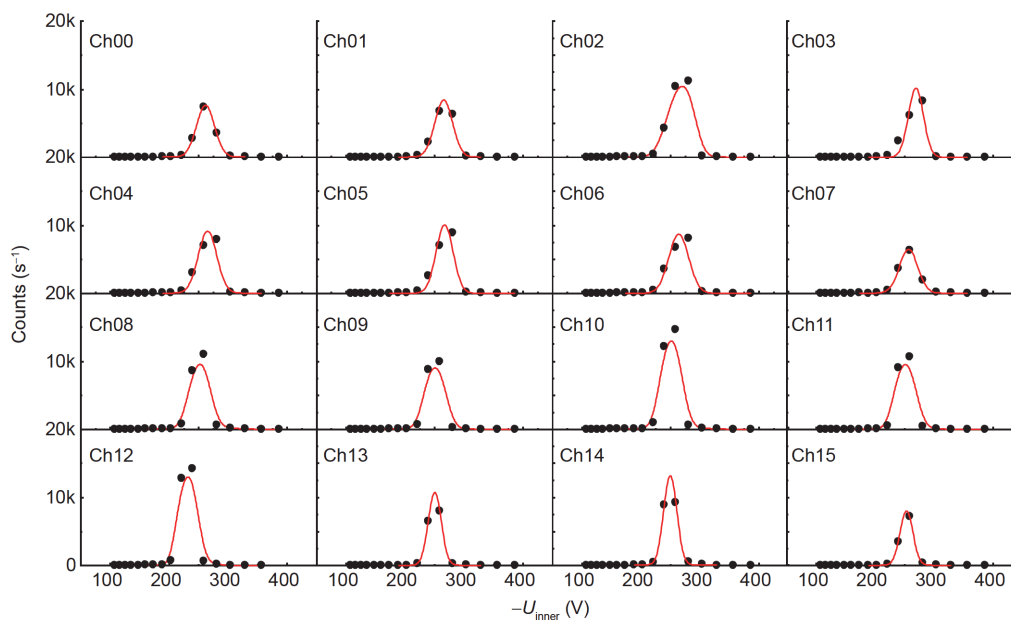


Figure 9 (Color online) Raw data of the energy responses for 16 azimuth angle channels obtained at a given energy of 1554 eV.

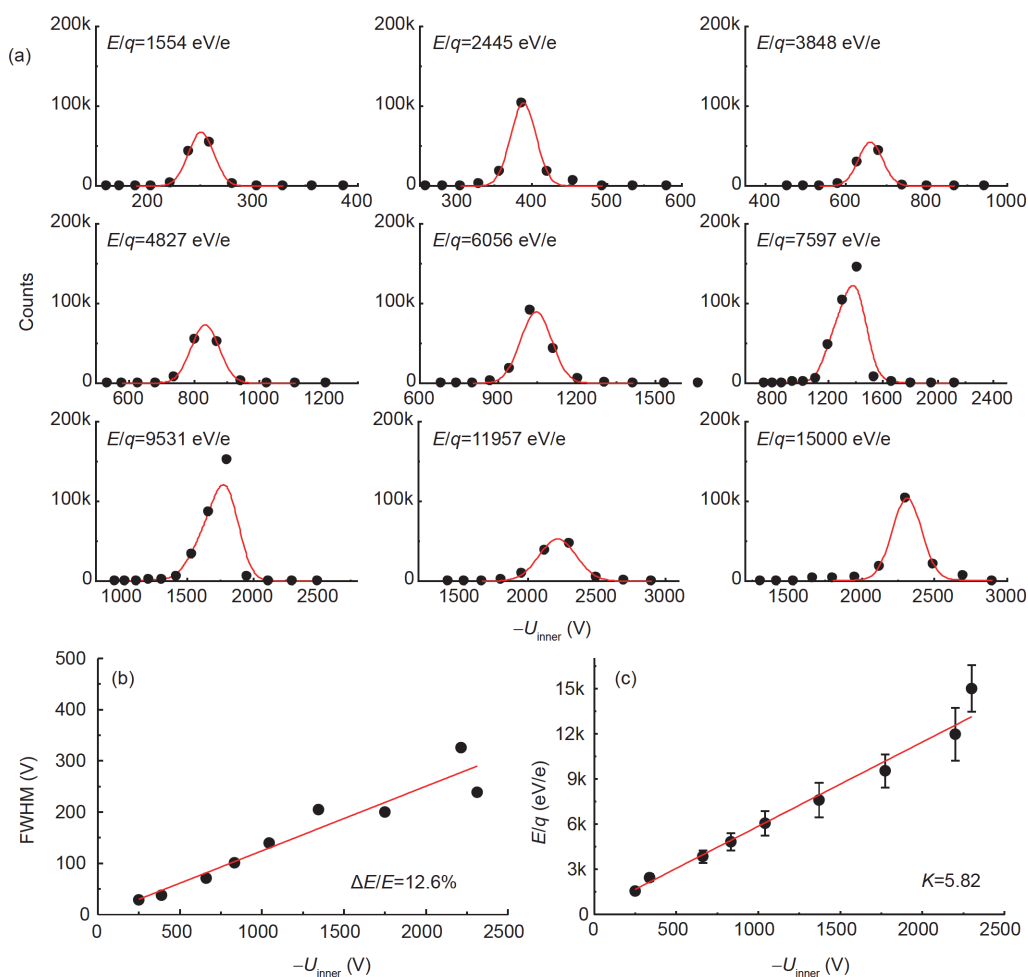


Figure 10 (Color online) (a) Energy response spectra; (b) energy resolution ratios; (c) analyzer constant obtained at a series of separate energies for one of azimuth angle channels (Ch08). The error bars in (c) represent the energy resolutions measured at the specific ion energies.

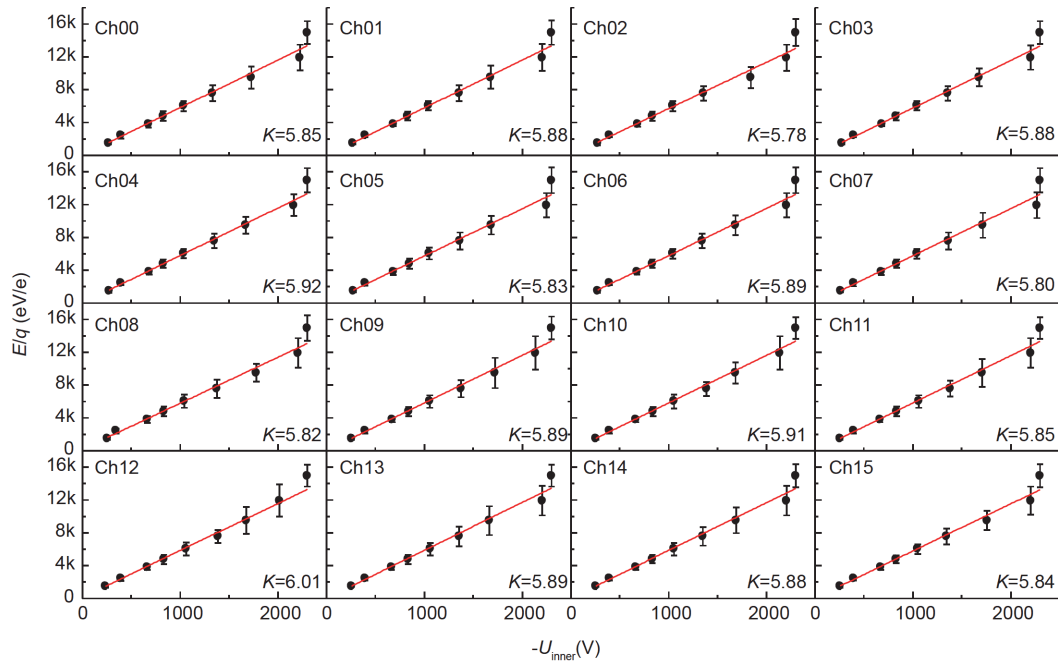


Figure 11 (Color online) Analyzer constant K for 16 azimuth angle channels obtained at a series of given energies, in which the error bars in the figure represent the energy resolutions measured at the specific ion energies.

constant K keeps a good uniformity for different energy and azimuth angle, and the value is close to the simulated value of 5.93.

6.2 Working with entrance deflection

For this working mode, the voltages applied to entrance deflectors and the inner sphere electrodes are scanning synchronously as Figure 8 shown. In the experiment, the elevation angle varies by rotating the LEIS through the 3-axis turntable. But due to the limitation of this turntable, the elevation angle can only change from -30° to 30° . In addition, due to the limited beam time, we only measured the energy-angle response spectra at 9 different elevation angles and the proton energy of 7597 eV. Figure 12 shows the elevation angle spectra, the relation between elevation angle and deflection voltage, and the normalized GF at the elevation angle β from -26° to 26° with the interval 6.5° . It's easy to find out from Figure 12(a) that β angle resolution is better than 8° . More importantly, the relation between elevation angles and deflection voltages are obtained from β response spectra, as shown in Figure 12(b). It shows that the relation can be fitted well by a linear function, i.e.,

$$\beta = 97.38 \frac{U_{\text{def}}}{E/q} + 2.5, \text{ which is well agreed with the result}$$

$\beta = 99.82 \frac{U_{\text{def}}}{E/q} + 1.96$ in simulation. In addition, the normalized GF factors at 9 different elevation angles, as shown in Figure 12(c), are derived according to the measured angular spectra. The behavior of these GF factors varied with

the elevation angles is in general consistent with the simulation as Figure 6(c) showed. Besides, the absolute GF can be estimated by the measured count rate at one elevation angle for one azimuth channel. As an example, one test shows that the beam current input into the entrance along $\beta=0$ and towards Ch08 anode of 22.5° is about 1.6 picoampere as monitored by the FC, which corresponds to the incident proton counts of about $5.6 \times 10^5 \text{ s}^{-1} \text{ mm}^{-2}$. From the central panel in Figure 12(a), the measured count rate at $\beta=0$ is about $2.3 \times 10^4 \text{ s}^{-1}$. Considering the active area ($A_e = 40.8 \text{ mm}^2$) of analyzer aperture, the absolute GF is estimated to be $\sim (1.0 \pm 0.2) \times 10^{-3}$, which includes the MCP efficiency and the transmittance of two Molybdenum grids. The simulated GF for each anode channel ($\sim 0.9 \times 10^{-3}$ after modification by considering the efficiencies of typically 60%–80% for MCP [25] and 90% for one grid) is in good accordance with the result estimated from calibration experiment. All the instrumental parameters are also listed in Table 1 for comparison.

7 Conclusions and future improvements

In this article, we report a low-energy ion spectrometer (LEIS) developed for use aboard three-axis stabilized spacecraft. Angular scanning deflectors are supplemented into a cylindrically symmetric top-hat electrostatic analyzer to provide a half-space field of view as $360^\circ \times 90^\circ$. It enables us to measure three-dimensional energy per charge distributions of space ions with good energy-, angular- and

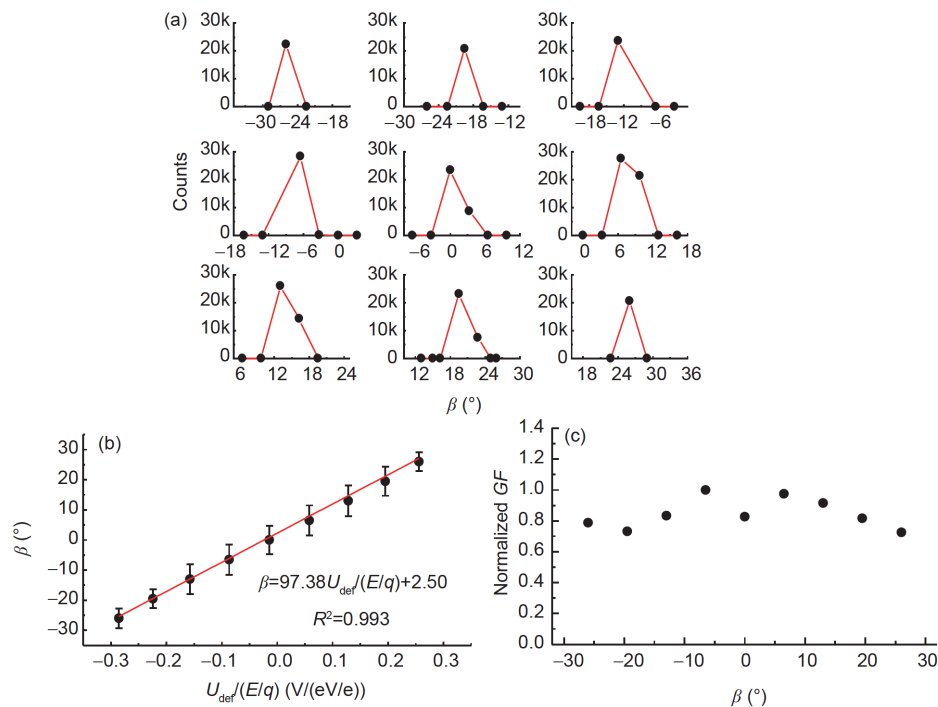


Figure 12 (Color online) (a) Elevation angle spectra; (b) the relation between deflection voltages and elevation angles; (c) the normalized GF for different elevation angles.

temporal-resolutions. We have designed and fabricated the LEIS flight model for detecting magnetospheric ions in geosynchronous orbit. The performance of this payload have been evaluated in detail by a series of simulation and environmental tests, and also been calibrated through laboratory experiments using a low-energy ion source. Good instrumental resolutions are achieved for the energy resolution ratio of better than 13% and the elevation resolution of better than 8° . Furthermore, the important relations between ion energies, elevation angles and deflection voltages of entrance and sphere electrodes are determined, together with the geometric factor representing the instrumental sensitivity. Consistency of the parameters obtained from simulation and calibration experiment shows the reliability and stability of the LEIS spectrometer. These results show that capabilities of the LEIS payload are in accordance with and even beyond the requirements of the mission. This instrument was equipped as a scientific payload onto the SJ-18 satellite of China and passed through a series of tests with the satellite. Unfortunately, the satellite launch was unsuccessful due to the rocket fault. Now the same instrument will be deployed onto a Chinese BD satellite on the geosynchronous orbit, which is scheduled to be launched in 2019.

The low energy ion spectrometer, particularly having the large FOV, is one of key instruments to detect the space plasma on a three-axis stabilized spacecraft. More and more missions will adopt it in the future. For further improvement of the instrument in this kind, we think that several following

points should be focused on: (1) further optimizations about structure should be done to improve the resolution of analyzer and angular uniformity. (2) HV power supplies should be improved to increase the maximum of voltage outputs, then we can extend the measurable energy and elevation angle ranges. (3) The FOV of analyzer should be optimized so that it would not be blocked by satellite itself.

This work was supported by the National Natural Science Foundation of China (Grant No. 41327802), the CAS Key Research Program of Frontier Sciences (Grant No. QYZDB-SSW-DQC015). The authors would like to thank engineers SUN ShuKun, SHI YuFeng, YANG HaiFeng, XIAO Jun-Qiang, ZHANG YuTu, WANG Hui, TANG Yong, XIE Qiong and other people from the Shandong Institute of Space Electronic Technology and China Academy of Space Technology for their help in the fabrication and environmental tests of this payload. We also would like to thank professors ZHU XiaoLong and MA XinWen from the Institute of Modern Physics, CAS for their valuable assistance in the calibration experiment.

- Carlson C W, Curtis D W, Paschmann G, et al. An instrument for rapidly measuring plasma distribution functions with high resolution. *Adv Space Res*, 1982, 2: 67–70
- Young D T, Bame S J, Thomsen M F, et al. 2π radian field of view toroidal electrostatic analyzer. *Rev Sci Instrum*, 1988, 59: 743–751
- Lin R P, Anderson K A, Ashford S, et al. A three-dimensional plasma and energetic particle investigation for the wind spacecraft. *Space Sci Rev*, 1995, 71: 125–153
- Rème H, Cotin F, Cros A, et al. The giotto electron plasma experiment. *J Phys E: Sci Instrum*, 1987, 20: 721
- Barabash S, Sauvaud J A, Gunell H, et al. The analyser of space plasmas and energetic atoms (ASPERA-4) for the venus express mission. *Planet Space Sci*, 2007, 55: 1772–1792
- Reme H, Bosqued J M, Sauvaud J A, et al. The cluster ion spectro-

- metry (CIS) experiment. *Space Sci Rev*, 1997, 79: 303–350
- 7 Rème H, Aoustin C, Bosqued J M, et al. First multispacecraft ion measurements in and near the earth's magnetosphere with the identical cluster ion spectrometry (CIS) experiment. *Ann Geophys*, 2001, 19: 1303–1354
 - 8 Carlson C W, McFadden J P, Turin P, et al. The electron and ion plasma experiment for fast. *Space Sci Rev*, 2001, 98: 33–66
 - 9 Young D T, Berthelier J J, Blanc M, et al. Cassini plasma spectrometer investigation. *Space Sci Rev*, 2004, 114: 1–112
 - 10 Barabash S, Lundin R, Andersson H, et al. The analyzer of space plasmas and energetic atoms (ASPERA-3) for the Mars Express Mission. *Space Sci Rev*, 2006, 126: 113–164
 - 11 Daglis I A, Thorne R M, Baumjohann W, et al. The terrestrial ring current: Origin, formation, and decay. *Rev Geophys*, 1999, 37: 407–438
 - 12 Jordanova V K, Kistler L M, Kozyra J U, et al. Collisional losses of ring current ions. *J Geophys Res*, 1996, 101: 111–126
 - 13 Fok M C, Kozyra J U, Nagy A F, et al. Decay of equatorial ring current ions and associated aeronomical consequences. *J Geophys Res*, 1993, 98: 19381–19393
 - 14 Miyoshi Y, Kataoka R. Ring current ions and radiation belt electrons during geomagnetic storms driven by coronal mass ejections and corotating interaction regions. *Geophys Res Lett*, 2005, 32: L21105
 - 15 Gary S P, Thomsen M F, Yin L, et al. Electromagnetic proton cyclotron instability: Interactions with magnetospheric protons. *J Geophys Res*, 1995, 100: 21961–21972
 - 16 Su Z, Wang G, Liu N, et al. Direct observation of generation and propagation of magnetosonic waves following substorm injection. *Geophys Res Lett*, 2017, 44: 7587–7597
 - 17 Horne R B, Thorne R M, Glauert S A, et al. Electron acceleration in the Van Allen radiation belts by fast magnetosonic waves. *Geophys Res Lett*, 2007, 34: L17107
 - 18 Yang C, Su Z, Xiao F, et al. A positive correlation between energetic electron butterfly distributions and magnetosonic waves in the radiation belt slot region. *Geophys Res Lett*, 2017, 44: 3980–3990
 - 19 Su Z, Gao Z, Zhu H, et al. Nonstorm time dropout of radiation belt electron fluxes on 24 September 2013. *J Geophys Res Space Phys*, 2016, 121: 6400–6416
 - 20 Funsten H O, Skoug R M, Guthrie A A, et al. Helium, Oxygen, Proton, and Electron (HOPE) mass spectrometer for the radiation belt storm probes mission. *Space Sci Rev*, 2013, 179: 423–484
 - 21 Spence H E, Reeves G D, Baker D N, et al. Science goals and overview of the radiation belt storm probes (RBSP) energetic particle, composition, and thermal plasma (ECT) suite on NASA's Van Allen probes mission. *Space Sci Rev*, 2013, 179: 311–336
 - 22 Mann I R, Lee E A, Claudepierre S G, et al. Discovery of the action of a geophysical synchrotron in the Earth's Van Allen radiation belts. *Nat Commun*, 2013, 4: 2795
 - 23 Collinson G A, Dorelli J C, Avakov L A, et al. The geometric factor of electrostatic plasma analyzers: A case study from the fast plasma investigation for the magnetospheric multiscale mission. *Rev Sci Instrum*, 2012, 83: 033303
 - 24 Knudsen D J, Burchill J K, Berg K, et al. A low-energy charged particle distribution imager with a compact sensor for space applications. *Rev Sci Instrum*, 2003, 74: 202–211
 - 25 Straub H C, Mangan M A, Lindsay B G, et al. Absolute detection efficiency of a microchannel plate detector for kilo-electron volt energy ions. *Rev Sci Instrum*, 1999, 70: 4238–4240